Bull. Chem. Soc. Ethiop. **2025**, 39(5), 987-1000.
DOI: https://dx.doi.org/10.4314/bcse.v39i5.13

ISSN 1011-3924
Printed in Ethiopia
Online ISSN 1726-801X

STURCTURE, CHARACTERIZATION AND COMPUTATION OF 1,1'-DIBENZYL-[4,4'-BIPYRIDINE]-1,1'-DIIUM NITRATE

Jia-Jun Wang[1,4*], Xu Cheng[2] and Chao-Hui Zhang[3*]

[1]Key Laboratory of Preparation and Applications of Environmental Friendly Materials of Ministry of Education, Jilin Normal University, Changchun, China
[2]Changchun No. 8 High School, Changchun, China
[3]School of Medical Information Engineering, Shenyang Medical College, Shenyang, China
[4]College of Chemistry, Jilin Normal University, Siping, China

(Received December 9, 2024; Revised January 27, 2025; Accepted January 28, 2025)

ABSTRACT. 1,1'-Dibenzyl-[4,4'-bipyridine]-1,1'-diium nitrate [named benzyl viologen (BV) dianions]'s structure analysis reveals it crystallized in the monoclinic system with a $P2_1/c$ space group, and each pyrdine N atom fused on a benzyl group and the N atom become a positive monovalent cation, the counter nitrate cations are lie at the two sides of the structure. In the crystal lattice, there are C-H···O hydrogen bonds and the π···π stacking interactions. The weak C–H···O hydrogen bond interactions demonstrated in the d_e surface and d_{norm}-surface of the Hirshfeld surface analysis. The IR spectrum were tested. The NMR spectra reveal the structure is accordance with the crystal structure. The computed molecular orbitals shown the HOMO electron cloud is mainly located at the benzene ring. The AIM analysis shows that the ρ_{BCP} and $\nabla^2\rho_{BCP}$ value is calculated for the C–H···O hydrogen bond interactions, and the interaction belongs to the typical closed-shell interactions. The molecular docking study shows the lowest binding energy is -5.28 kcal/mol, the interaction between BV and Lys dominated by hydrophobic interactions.

KEY WORDS: Benzyl viologen, Hirshfeld surface analysis, AIM, Molecular docking

INTRODUCTION

Crystal engineering based on organics [1] have been fast developing in the last few years. The organic crystals have already applied in all aspects of life. Their potential applications including such as the organic optic-electric device [2], and luminescence [3], etc.

1,1'-Dibenzyl-[4,4'-bipyridine]-1,1'-diium nitrate, named benzyl viologen (BV) dianions are the useful substances. Benzyl viologen dianion has been used as extramicellar probe luminescence to monitor association of cations to the micelle [4]. The trifluoromethyl substituents of benzyl-based viologen have the electrochromic performance, the stability of viologen based electrochromic device was significantly reduced by the dimer formation, and the resultant aggregation of viologens, which may occur once viologen dication (V^{2+}) was reduced to viologen radical cation ($V^{+\cdot}$) [5]. The viologen derivatives' energy bands matched photocatalysis enhancement that is based on their electron-transfer-mediator [6]. Otherwise, the benzyl viologen also has a certain toxic to living organisms [7].

The hydrogen bonds and π-π interactions are critical in chemistry and life science [8]. The Hirshfeld surface analysis (HS) [9] and the atom in molecule (AIM) theory [10] are the effective means to research hydrogen bonds from different aspects. The Hirshfeld sufaces analysis utilized to identify a type and region of intermolecular interactions (which contains the hydrogen bonds). Hirshfeld surface analyses comprises d_{norm}- and shape index surfaces, and 2D fingerprint plots (FP). The AIM theory also can analyze the properties of hydrogen bonds. In AIM view, the main concept is the bond critical points (BCP), they are the evidence of hydrogen bond is the existence of a bond path and a BCP between the donor hydrogen and the acceptor. Researcher also

*Corresponding authors. E-mail: jiajunwang@jlnu.edu.cn and chzhang@symc.edu.cn

developed the criteria for the assessment of the hydrogen bonds [11]. Nowadays, molecular docking has used for understanding the principles by which small-molecule ligands recognize and interact with macromolecules is of great importance in pharmaceutical research and development [12].

In this paper, we synthesized a benzyl viologen (BV) dinitrate, characterized it by X-ray single crystal diffraction, elemental analysis, infrared spectroscopy and NMR. We performed the Hirshfeld surface analysis, and calculated the molecular orbitals. We executed the atoms in molecules (AIM) analysis, also researched the molecular docking.

EXPERIMENTAL

Preparation of crystal

Benzyl chloride 0.10 mol (12.60 g) and 4,4'-bipyridine 0.10 mol (15.60 g) dissolved in 60 mL DMF, and then heated to 100 °C with stirring for 1.5 h, due to the strong reactive activity of benzyl chloride, two moles benzyl chloride undergo the electrophilic substitution reaction with one mole bipyridine, and we get the bi-substituted product, after cooled to room temperature, put the reaction mixture to the refrigerator and keep the temperature about 0 °C for 4 h, then filtered and washed with cold anhydrous ethanol 2 times. After dried we get white solid powder 9.41 g (yield 20.3 %), this solid is benzyl viologen dichloride. The 1.00 g solid powder solved in a 16 mL 2 mol/L solution of $Co(NO_3)_2$ (as the source of nitrate ion), we stay it for one week, after that the light pink crystals formed (0.24 g), which is the title compound benzyl viologen dinitrate (yield 21%, the synthetic strategy is shown in Scheme 1). Then we choose the suitable crystal for X-ray diffraction. The C, H and N contents determined by elemental analysis: calcd. (%) for $C_{24}H_{22}N_4O_6$: C, 62.33; H, 4.79; N, 12.11; found (%): C, 61.69; H, 4.52; N, 11.87. IR (cm^{-1}): 3447(s), 3127(s), 3061(s), 2350(m), 1835(w), 1737(w), 1637(s), 1559(m), 1499(m), 1446(s), 1381(s), 1316(s), 1221(s), 1155(m), 1036(m), 920(w), 847(m), 806(m), 745(s), 699(m), 664(w), 614(m), 550(w), 465(w), 444(w), 400(w).

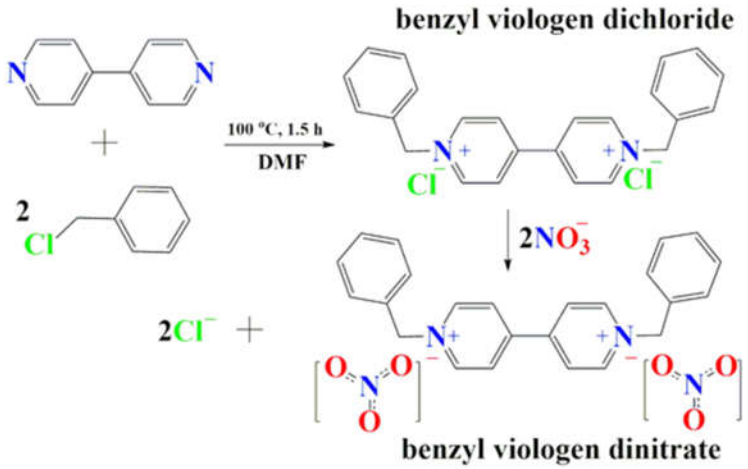

Scheme 1. The synthetic route of BV dinitrate.

Structure determination and physical measurements

A colorless block crystal for the compound with dimensions of 0.21 mm × 0.20 mm × 0.19 mm was chosen for X-ray diffraction analysis. Crystal structure measurement was performed on a Ragaku XtaLAB Pro diffractometer by using ω scan mode at 293(2) K. Absorption corrections were applied with a multi-scan mode [13]. A total of 8543 reflections were obtained in the range of $5.30 \leq \theta \leq 29.91^{\circ}$, of which 2781 were independent (R_{int} = 0.0313) and 2823 observed reflections with $I > 2\sigma(I)$ were employed for structure determination and refinement. The structure was solved by direct methods with SHELXT [14] and refined by full-matrix least-squares techniques using SHELXL-2018 [15] within Olex2 [16]. All non-hydrogen atoms were refined anisotropically. All H atoms on C atoms were positioned geometrically and refined as riding. The final R = 0.0660, wR = 0.1799 ($w = 1/\sigma^2(F_o^2)+(0.0913P)^2+0.5934P$] where $P = (F_o^2 + 2F_c^2)/3$), $(\Delta/\sigma)_{max}$ = 0.000, S = 1.071, $(\Delta\rho)_{max}$ = 0.859 and $(\Delta\rho)_{min}$ = –0.526 e/Å^3. Crystallographic data for the structure in this work has been deposited with a copy of the data and is freely available by reference to deposit number (CCDC: 2281830). There are two B level alerts in the checkCIF files: For complex: (i) PLAT097_ALERT_2_B: Large reported max. (Positive) pesidual density 0.86 eÅ^{-3}. This issue of alert level B caused a residual density maximum larger. This is caused by the disorder of the nitrate ion, the residual density is not very large and it is acceptable. (ii) PLAT910_ALERT_3_B: The missing FCF reflections below theta (min) were caused by the high beamstop theta (min) limit set and large unit cell, and so on. The molecular graphics was prepared using program Diamond 3.1c [17]. The elemental analysis performed on a EurVector EA3000 elemental analyzer. The FTIR spectrum recorded at room (298 K) on a Thermo Fisher Nicolet 6700 FTIR spectrometer in the range of 4000–400 cm^{-1}. The NMR tested on a Bruker AVANCE III HD 400M spectrometer. Other reagents were of analytical grade.

Theoretical methods

The calculations were performed for the compound, and the optimization with Gaussian 16 program [18] at the ωB97XD [19, 20] level (includes dispersion correction), the 6-31++g(d) [21] basis set for C, H, O, N. For modeling the initial guess of BV dinitrate was obtained from the X-ray refinement data (cif) and optimized the structure. The solvent effects were included by applying the self-consistent reaction field (SCRF) and solvation model based on density (SMD) [22] options within the program when optimizing the structure, we utilized the solvent model to instead the gas model, and using the keyword: "scrf = (smd, solvent = water)".

In AIM calculation, when selecting model, we select a nitrate anion and four BV^{2+} cations that around it to consist a heptavalent cation (this configuration consists all the five kinds of hydrogen bonds), and use it to represent the crystal surroundings in the calculation. In which it exhibited the hydrogen bonds, for ensuring the calculated hydrogen bonds are consistent with the crystal structure. We directly using the crystal structure and computed the single point (not using the opted structure) to get the fchk file. The method and the basis sets are: "wb97xd/6-311++G(d) SP scrf = (smd, solvent = water)", finally, we use the Multiwfn program [23] to research the topological properties of the bonds of BV dinitrate. The specific operating steps are: (1) Launch the multiwfn software (v 3.8) by double click the multiwfn.exe and load the fchk file though drag the fchk file or input file path. (2) Input 2 and press enter key (2: Topology analysis). (3) Select 2, press enter; then in turn select 3,4,5,7, 8,9 (2: Search CPs from nuclear positions; 3: Search CPs from midpoint of atomic pairs; 4: Search CPs from triangle center of three atoms; 5: Search CPs from pyramid center of four atoms; 7: Show real space function values at specific CP or all CPs; Hint: after input 7 and press enter, the software ask you continue enter the index of the CP, and you can input 0, and the properties of all CPs will be outputted to CPprop.txt. 8: Generating the paths connecting (3,-3) and (3,-1) CPs; 9 Generating the paths connecting (3,+1) and (3,+3)

CPs.).

RESULTS AND DISCUSSION

Crystal structure description

The structure of benzyl viologen (BV) dinitrate described in Figure 1(a) and Table 1. It crystallized in the monoclinic system with a $P2_{1/c}$ space group, the lattice constants a = 6.3633(8) Å, b = 13.1291(17) Å, c = 13.1486(14) Å, and β = 94.603(11)°. We can see each pyrdine N atom fused on a benzyl group and the N atom become a positive monovalent cation; the counter nitrate cations are lie at the two side of the structure. The C7-N1 distance is 1.500 Å, the C6-C7 distance is 1.504 Å, the N1-C7-C6 angle is 112.25°, and the dihedral angle between benzene plane (contains atoms C1 to C6) and the pyridine ring plane (contains atoms N1, C8 to C12) is 105.73°.

In crystal lattice, there are C−H···O hydrogen bonds (the C11−H11···O2$^{\#1}$, C12−H12···O1$^{\#2}$, C7−H7A···O1$^{\#3}$, C7−H7B···O1$^{\#2}$ and C9−H9···O2$^{\#4}$, in Table 2) and the π···π stacking interactions as color circle displayed in Figure 1(b). The distances between the center of gravity for the rings are 3.808 Å [Cg(1)···Cg(2)^{P} and Cg(2)···Cg(1)^{Q}] and 3.925 Å [Cg(2)···Cg(2)^{R}, symmetry code, P = x, 3/2-y, 1/2+z; Q = x, 3/2-y, -1/2+z; R = 1-x, 1-y, 1-z].

Table 1. Crystal and refinement data obtained for BV dinitrate.

CCDC	2281830	Name	Benzyl viologen dinitrate
Empirical formula	$C_{24}H_{22}N_4O_6$	μ/mm^{-1}	0.103
Formula weight	462.45	F(000)	484.0
Crystal system	Monoclinic	Crystal size/mm^3	0.21 × 0.20 × 0.19
Space group	$P2_1/c$	Radiation	MoKα (λ = 0.71073)
a/Å	6.3633(8)	2Θ range for data collection/°	10.594 to 59.824
b/Å	13.1291(17)	Index ranges	$-8 \le h \le 8$, $-16 \le k \le 17$, $-16 \le l \le 17$
c/Å	13.1486(14)	Reflections collected	8543
α/°	90	Independent reflections	2781 [R_{int} = 0.0313, R_{sigma} = 0.0369]
β/°	94.603(11)	Data/restraints /parameters	2781/0/159
γ/°	90	Goodness-of-fit on F^2	1.071
Volume/Å^3	1094.9(2)	Final R indexes [I>2σ (I)]	R_1 = 0.0660, wR_2 = 0.1799
Z	2	Final R indexes [all data]	R_1 = 0.0928, wR_2 = 0.2033
ρ_{calc}g/cm^3	1.403	Largest diff. peak/hole /e Å^{-3}	0.86/-0.53

Table 2. Hydrogen bonds of the BV dinitrate.

D−H···A	D−H (Å)	H···A (Å)	D···A (Å)	D−H···A (°)
C11−H11···O2$^{\#1}$	0.93	2.41	3.325(3)	168.4
C12−H12···O1$^{\#2}$	0.93	2.47	3.344(3)	156.7
C7−H7A···O1$^{\#3}$	0.97	2.50	3.327(3)	143.2
C7−H7B···O1$^{\#2}$	0.97	2.53	3.452(3)	158.6
C9−H9···O2$^{\#4}$	0.93	2.39	3.299(3)	165.1

#1: -x, 1-y, 2-z; #2: -x, 1/2+y, 3/2-z; #3:1-x, 1/2+y, 3/2-z; #4: 1+x, +y, +z.

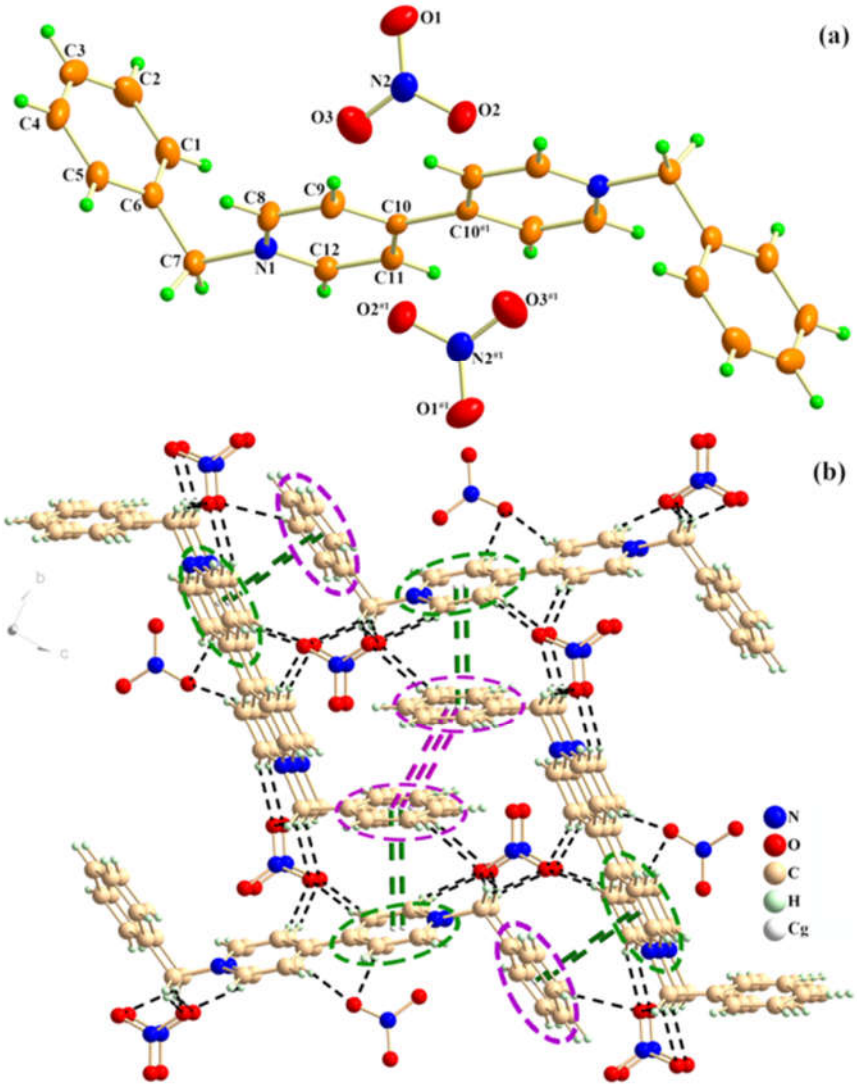

Figure 1. (a) The structure of BV dinitrate. (Drawn at 30% ellipsoid contour probability level, symmetry code #1: 1-x, 1-y, 2-z). (b) The C-H···O hydrogen bonds (black dotted lines), π···π interactions [pink (Cg(2)···Cg(2)) dotted lines and green (Cg(1)···Cg(2)) dotted lines] of BV dinitrate. The green oval dashed box represent for 6-membered ring (1): N(1) → C(8) → C(9) → C(10) → C(11) → C(12) →; The pink oval dashed box represent for 6-membered ring (2) C(1) → C(2) → C(3) → C(4) → C(5) → C(6) →; The white ball Cg represent for the center gravity of the ring.

Hirshfeld surface analysis

In recent years the analysis of molecular crystal structures using software based on Hirshfeld surfaces has become into fashioned [24, 25], they were performed calculated and drawn using CrystalExplorer software [26]. Hirshfeld surface analysis comprising curveness surface, d_e surface, d_{norm}- and shape index-surfaces, and 2D fingerprint plots (FP).

As shown in Figure 2(a), the hydrogen bonds result in red spots near the hydrogen bonds acceptor and donor atoms in d_{norm} surfaces, while hydrogen bonds result in red and yellow spots spots in d_e surfaces.

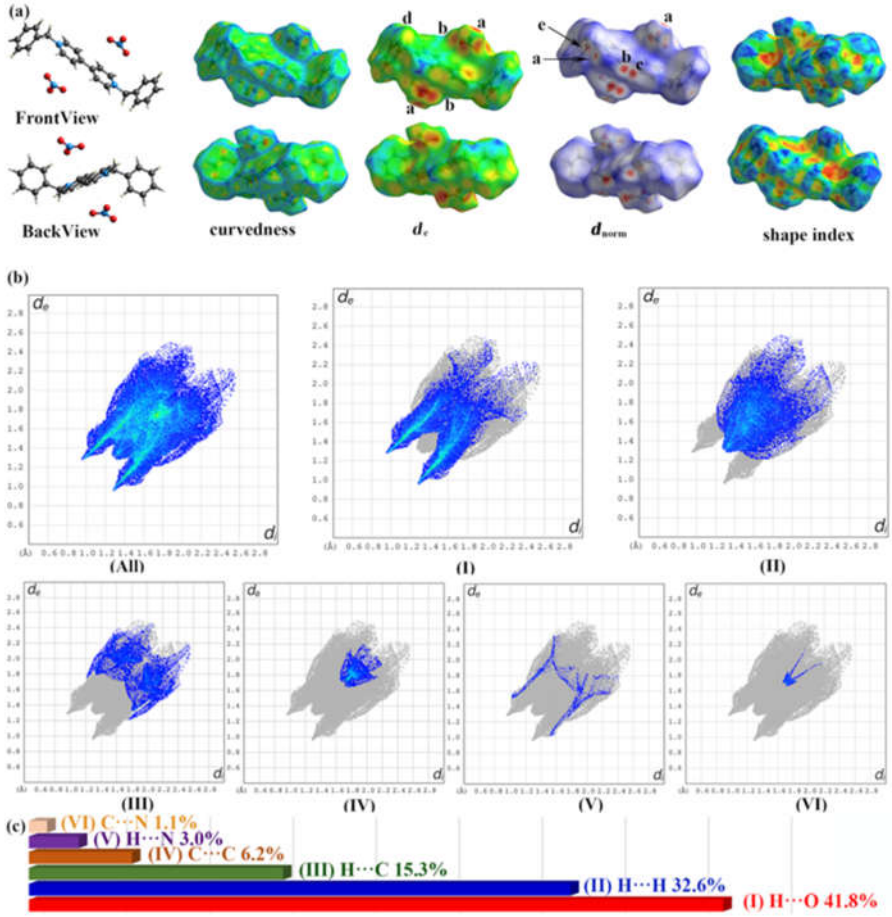

Figure 2. The Hirshfeld surface analysis of the BV dinitrate. (a) The curveness surfaces, d_e surfaces, d_{norm} surfaces and shape-index surfaces mapped on Hirshfeld surface. (b) 2D fingerprint plots for BV dinitrate (d_i is the closest internal distance from a given point on the Hirshfeld surface and d_e is the closest external contacts). (c) The relative contributions of the intermolecular interactions.

The weak C–H···O hydrogen bond interactions in the compound demonstrated in the d_e surface and d_{norm}-surface. It can be seen that spot "a" correspondences to C12−H12···O1. The spot "b" correspondences to C11-H11···O2. The spot "c" correspondences to C9-H9···O2. The pale yellow spot "d" on d_e surface correspondences to C7−H7A···O1 and the faint red spot on d_{norm} surface correspondences to C7−H7B···O1.

By observing the fingerprint plot (Figure 2(b)), we attempt quantitatively analyze the significant intermolecular interactions in the crystal structure. The H···O intermolecular interactions in the compound, appeared as two distinct long sharp spikes in the FP, at $d_i + d_e \approx 0.95 + 1.25 = 2.20$ Å, which is roughly close to the observed hydrogen bonds' H···O distance of 2.39~2.53 Å (Table 2). In this molecule, there are two spikes appear at (d_i, d_e) ≈ (0.95 Å, 1.25 Å) and (d_e, d_i) ≈ (1.25 Å, 0.95 Å, Figure 2(b)), and the spikes appear in the same manner.

The C···C close contacts appear as a blunt spike at (d_e, d_i) ≈ (1.70 Å, 1.70 Å) in the FP, occurring at $d_i + d_e \approx 3.40$ Å, it appear as the spike at $d_i + d_e$ distances are close to the Cg···Cg distances in crystal (3.81, 3.92 Å, Figure 2 (b)). It corresponds to the π···π stacking interactions. The relative contributions of the intermolecular interactions to the Hirshfeld surface for the compound were calculated (the bar diagram in Figure 2(c)). The greatest contribution (41.8 %) is from H···O contacts, after that it is the H···H contacts (32.6 %), and H···C/C···H contacts is 15.3 %, then the C···C contacts (which is stands for the π···π intermolecular interactions, 6.2 %), the contribution from the H···N/N···H contacts is 3.0 %, finally, the C···N contacts is 1.1 %.

Infrared spectroscopy

The strong vibrations at 3127 cm^{-1} attributed to the C-H stretching vibration of benzene ring [27]. The vibrations at 1737 cm^{-1} may ascribed to the C-C stretching vibration of dipyridine ring. The vibrations at 1637 cm^{-1} may be due to the inplane antisymmetric stretching vibration of the dipyridine ring. The vibrations at 1559 cm^{-1} may cause by the inplane symmetric stretching vibration of the dipyridine ring. The vibrations at 1499 and 1446 cm^{-1} may be caused by the symmetric and antisymmetric stretching vibrations of the nitrate ion. The vibrations at 1381 cm^{-1} may be because the rocking vibration of the dipyridine ring and the symmetric strenching vibration of nitrate ion. While the vibrations at 745 and 699 cm^{-1} may the C-H antisymmetric stretching vibrations of the benzene rings.

NMR spectra

From Figure 3(a), we can see there are sharp peaks on the spectrum, the peak's the chemical shift (δ) sited at 0.0 is the reference material (TMS), and the peaks at 2.51 and 3.39 ppm are the deuterated solvent DMSO and the trace amount of water in DMSO. The peak at 5.95 ppm is attribute to the methylene hydrogen atom (2H, -CH_2-). The peak at 7.46 ppm is hydrogen atoms of the substitute benzene ring, which is the meta-(*m*) and para-(*p*) site hydrogen atoms of benzene ring (3H). The peak at 7.61 ppm is also the hydrogen atoms of the benzene ring, which is the ortho-(*o*) site hydrogen atoms of benzene ring (2H). The peak at 8.76 ppm is the hydrogen atoms of the pyridine ring, which is the meta-(*m*) site hydrogen atoms of pyridine N atom (2H). The peak at 9.51 ppm is the hydrogen atoms of the pyridine ring, which is the ortho- (*o*) site hydrogen atoms of pyridine N on the pyridine ring (2H). The integration is 1:1.5:1:1:1, which is in accordance with the compound 2H:3H:2H:2H:2H.

Figure 3(b) suggested the chemical shift at 63.33 ppm is methylene CH_2-'s peak. The chemical shift at 127.08 ppm is attribute to the pyridine N's *meta* (*m*) site carbon atoms on the pyridine ring. The chemical shift at 128.76 ppm was corresponding to the substituted benzene ring's *meta*

(*m*) position carbon atom. The chemical shift at 129.13 ppm was due to the substituted benzene ring's *ortho* (*o*) site carbon atom. The chemical shift at 129.37 ppm was result of the substituted benzene ring's *para* (*p*) site carbon atom. While the chemical shift at 133.97 ppm was corresponding to the substituted benzene ring's *ipso* (*i*) site of the carbon atom. The chemical shift at 133.97 ppm was corresponding to the substituted benzene ring's *ipso* (*i*) site of the carbon atom' peak.

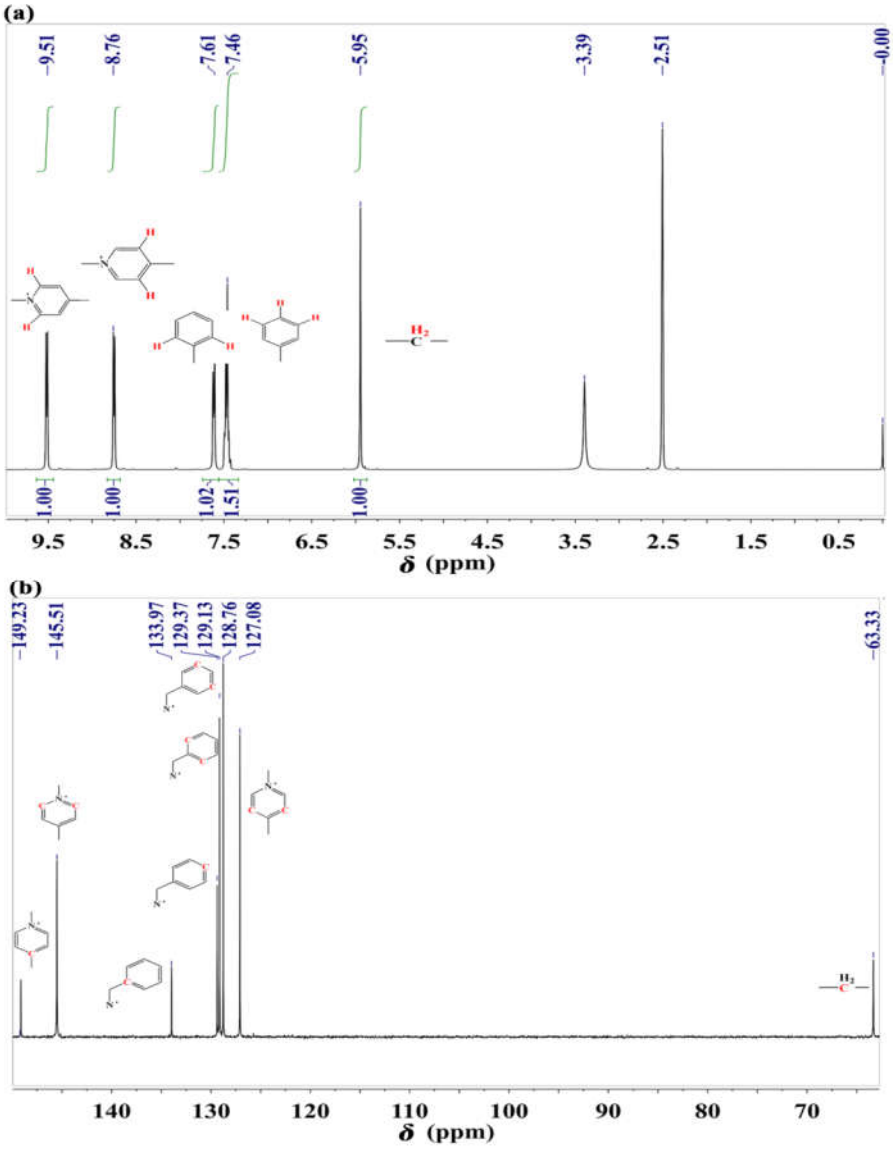

Figure 3. The ^{1}H (a) and ^{13}C (b) spectra of BV dinitrate in solvent DMSO-d_6.

Molecular orbital

For computing the electron cloud, the modeling the initial guess of BV dinitrate was obtained from the X-ray refinement data (cif). We opted the model neutral structure in calculation. The calculation covered 56 atoms, 242 electrons, 712 basis functions, 1198 primitive gaussians, 121 α electrons and 121 β electrons for the model of compound. As the model does not have a single electron, the spin multiplicity is 1. The total molecular energy is –1597.501 a.u., the energies of HOMO and LUMO are –0.334 and –0.046 a.u., respectively, with the ΔE(ELUMO–EHOMO) value to be –0.288 a.u., which shows the complound is stable [28] in ground state. The HOMO (H) and LUMO (L) of BV dinitrate, from Figure 4 we can see the LUMO electron cloud is mainly located at the 4,4'-bipyridine, and the HOMO electron cloud is mainly sited at the benzene ring.

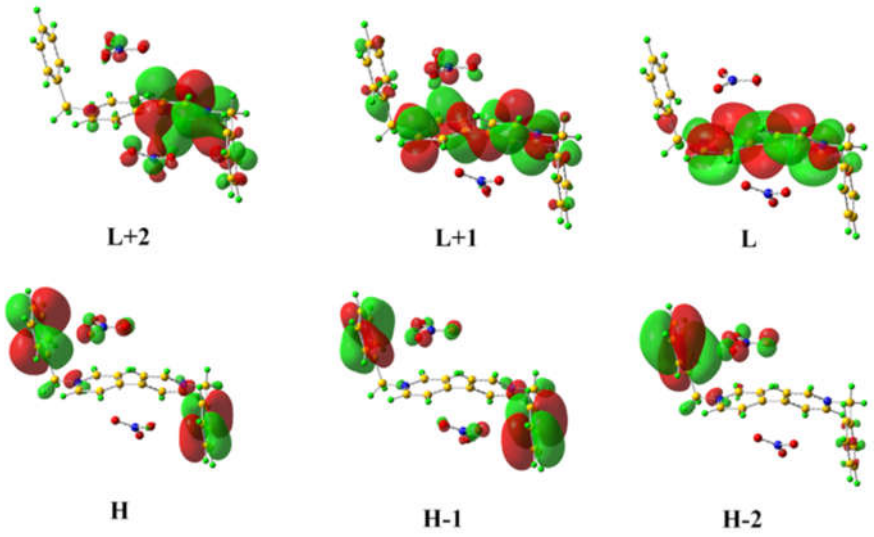

Figure 4. The HOMO and LUMO of BV dinitrate (H = HOMO, L = LUMO).

Atoms in molecules (AIM)

The topology analysis proposed by Bader was initially used for researching electron density in "atoms in molecules" (AIM) theory [10, 29]. In AIM theory, it based on the parameters at a bond critical point (BCP is the corresponding electron density analysis, position (3, -1)). Popelier insisted that the hydrogen bond's electron density at BCP (ρ_{BCP}) should be in the scope of 0.002–0.035 a.u. and the electron density Laplacian value ($\nabla^2\rho_{BCP}$) should be confined in the region from 0.024 to 0.139 a.u. [30].

The general view of Figure 5 shows the existence of a BCP in each hydrogen bond (C–H···O bond). The electron density (ρ_{BCP}) and Laplacian electron density ($\nabla^2\rho_{BCP}$) of BCP in the compound are listed in Table 3.

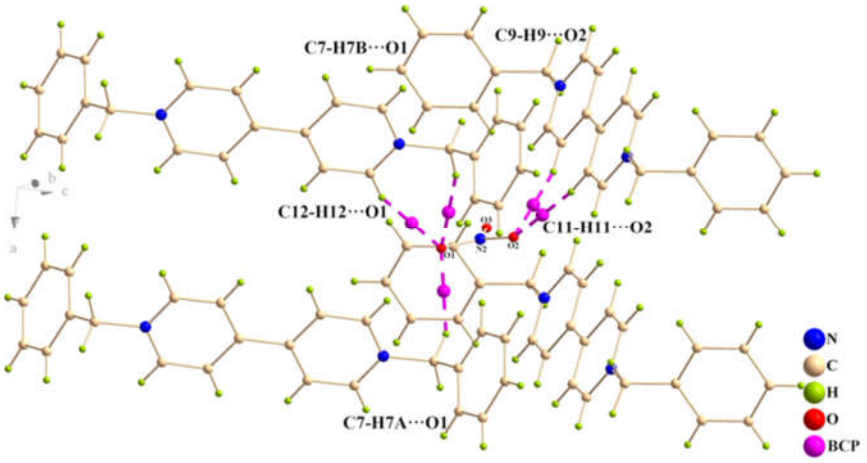

Figure 5. The abridged general view of hydrogen bonds BCP (pink ball) from the four quaternary model of the BV dinitrate. (Other BCPs were omitted for clarity).

The larger value of ρ_{BCP} and $\nabla^2\rho_{BCP}$ is found for the C–H···O, suggesting that hydrogen bond interaction are the stronger. The ρ_{BCP} value (from 0.008 to 0.011 a.u.) for the C–H ···O hydrogen bonds are all in the suggested interval of 0.002–0.035 a.u. [30, 31] for the hydrogen bond. The sum of Hessian matrix eigenvalues of electron density λ_1, λ_2, and λ_3 is $\nabla^2\rho_{BCP}$. The numeric value of $\nabla^2\rho_{BCP}$ for C–H···O interactions are in the region of 0.0285–0.0391 a.u. for hydrogen bonds. Bader et al. believed that for the closed-shell interactions, the $\nabla^2\rho_{BCP}$ value is positive [29, 32]. Clearly, based on Table 3, the C–H···O hydrogen bonds we studied are remained with the typical closed-shell interactions.

Table 3. The distance d(D···A), interaction energies (E_{int}), the electron density (ρ_{BCP}), the Laplacian of electron density ($\nabla^2\rho_{BCP}$), and the eigenvalues of Hessian at BCP (λ_1, λ_2 and λ_3) of BV dinitrate. And the local properties at BCP: the potential energy density, V(b), the Lagrangian kinetic energy density, G(b), as well as the total energy density H(b) of the title compound were computed at ωB97XD/6-311+G(d) level. The strength of bond, interaction energy (E_{int}), is obtained based on the electron density ρ_{BCP} fitting formula which usted the Lu *et al.* proposed fitting formula: $E_{int} = -223.08 \times \rho_{BCP} + 0.7423$ [33]. [The symmetry codes (#1, #2 and #3) are the same as Table 2. The unit of d is Å, the unit of E_{int} is kcal·mol^{-1}, $|V(b)/G(b)|$ is an ratio, no unit, other units are atom unit (a.u.).].

Interaction	C11–H11···O2$^{\#1}$	C12–H12···O1$^{\#2}$	C7–H7A···O1$^{\#3}$	C7–H7B···O1$^{\#2}$	C9–H9···O2$^{\#4}$
d(D···A)	3.325(3)	3.344(3)	3.327(3)	3.452(3)	3.299(3)
E_{int}	-1.1316	-0.9977	-1.221	-1.0647	-1.6000
ρ_{BCP}	0.0084	0.0078	0.0088	0.0081	0.0105
$\nabla^2\rho_{BCP}$	0.0353	0.0312	0.0309	0.0285	0.0391
λ_1	-0.0082	-0.0078	-0.0084	-0.0072	-0.0109
λ_2	-0.0074	-0.0070	-0.0077	-0.0061	-0.0105
λ_3	0.0509	0.0460	0.0470	0.0418	0.0604
V(b)	-0.0054	-0.0048	-0.0054	-0.0052	-0.0067
G(b)	0.0071	0.0063	0.0066	0.0062	0.0082
H(b)	0.0017	0.0015	0.0011	0.0010	0.0015
$\lvert V(b)/G(b)\rvert$	0.7606	0.7619	0.8182	0.8387	0.8171

Morrison [34], and Espinosa [35] *et al.* [36] suggested bond interactions are classified according to the $|V(b)|/G(b)$ ratio. The ratio $|V(b)|/G(b) < 1$, the bonded interaction is regarded as the closed shell, when $|V(b)|/G(b) > 2$, it is considered as the typically covalent interaction; and when $1 < |V(b)|/G(b) < 2$, it is the intermediate character. As it is presented in Table 3 , the mean Lagrangian kinetic energy density is a bit larger than the mean potential energy density for the C–H···O interactions. It brings about the total energy density $H(b)$ is drawn near to 0 and the $|V(b)|/G(b)$ ratio is in the range from 0.7606 to 0.8387, and it is less than 1.0. So, the C–H···O interactions are the closed shell for the model of the compound in another view of the perspective.

Molecular docking

Molecular docking is an efficient technique providing important information about the binding mechanism, affinity and activity of drug candidates to their protein targets such as lysozyme [37]. Lysozyme (Lys) is a small globular monomeric protein, the most widely studied one following human/bovine serum albumin. Lys is composed of 129 amino acid residues with six tryptophan (Trp), three tyrosine (Tyr) residues and four disulfide bonds and is known as a highly functional protein in our body system [38]. Lys shows antibacterial action by hydrolyzing the bond in the middle of Nacetylglucosamine and N-acetylmuramic acid of the bacterial cell wall. Hen egg Lys is 60% sequence homologous to human Lys [39] and is suitable for use as a model protein for studying protein-ligand interactions [37].

The molecular modeling study is performed on AutoDock 4.2 suite of programs [40]. The Lamarckian genetic algorithm (LGA) in AutoDock 4.2 is used to study the interaction between hen egg lysozyme (Lys) and BV. The Lys structure acquired from the RSCB Protein Data Bank (website: https://www.rcsb.org/, PDB ID 6LEV). Before docking, we removed four types of small molecules: NDP, EA0, PO_4^{3-} and water molecules. The protein contains chain A and chain B, we also removed the repeated B chain with PyMol molecular graphic system [41]. For docking study of Lys in the presence of BV ligand, ten independent docking runs carried out. The visualization of the docked position has been drawn with PyMol.

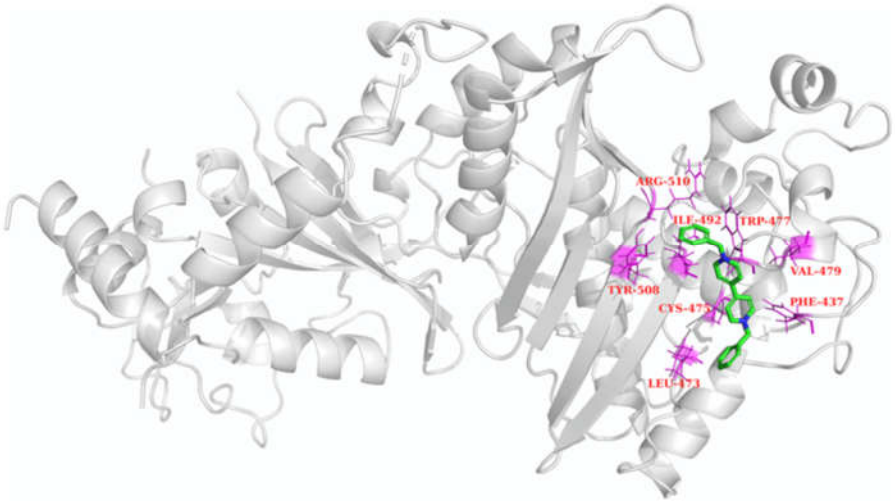

Figure 6. Docking interaction of Lys-BV binding.

The obtained docking result for Lys-BV interaction is given in Figure 6. In docking results, 10 conformers obtained and among which the conformer with the lowest binding free energy has found, and the lowest binding energy is -5.28 kcal/mol, the inhibition constant (K_i) is 135.11 μM and the RMSD Reference is 70.21. The BV molecule is surrounded by 8 amino acid residues of Lys within 4 Å (Figure 6), there are 5 hydrophobic residues (LEU473, PHE437, VAL479, TRP477 and ILE492) and 3 hydrophilic residues (CYS475, TYR508 and ARG510) [37]. Therefore, it may be conferred that the interaction between BV and Lys is dominated by hydrophobic interactions.

Generally, there are variances theoretical or empirical results as the X-ray structure of the protein from crystals is dissimilar from the aqueous system used, which affect the microenvironment of ligand [42]. Therefore, the results from docking studies can provide a suitable structural basis to correlate the experimental results of Lys-BV system.

CONCLUTION

We synthesized the 1,1'-dibenzyl-[4,4'-bipyridine]-1,1'-diium nitrate, and the structure analysis reveals it crystallized in the monoclinic system with a $P2_1/c$ space group. In the crystal lattice, there are C-H···O hydrogen bonds and the π···π stacking interactions. In Hirshfeld surface analysis, the weak C–H···O hydrogen bond interactions demonstrated in the d_e surface and d_{norm}-surface. The NMR spectra is accordance with the crystal structure.

The HOMOs of the compound are mainly located at the benzene ring. The AIM analysis shows that the ρ_{BCP} and $\nabla^2\rho_{BCP}$ value is found for the C–H···O hydrogen bond interaction. The ρ_{BCP} value (from 0.008 to 0.011 a.u.) for the C–H···O hydrogen bond. The numeric value of $\nabla^2\rho_{BCP}$ for C–H···O interactions are in the region of 0.0285–0.0391 a.u. for hydrogen bonds. They belongs to the typical closed-shell interactions, the $\nabla^2\rho_{BCP}$ value is positive. The molecular modeling study shows the lowest binding binding energy (of 10 conformers) is -5.28 kcal/mol. Moreover, the interaction between BV and Lys dominated by hydrophobic interactions. This research has some scientific merit in exploring BV compounds.

Conflict of interest

The authors declare no competing financial interest.

ACKNOWLEDGEMENTS

The authors thanks Hui Jiang of Jilin Agricultural Science and Technology University for X-ray diffraction structure measurement. This work was supported by Young Teacher's Scientific Research Ability Cultivation and Enhancement Program of Jilin Normal University [Grant No. 0521407].

REFERENCES

1. Mohammed, E.R.; Sulleman, I.A.; Saied, S.M.; Sabah, A.A. Synthesis of novel complexes derived from methyl or benzyl 4-amino antipyrinyl dithiocarbamtes with divalent Mn(II), Co(II), Ni(II), Zn(II) and Cu(II). *Bull. Chem. Soc. Ethiop.* **2025**, 39, 447-457.
2. Sergawie, A.; Admassie, S.; Mammo, W.; Yohannes, T.; Solomon T. Synthesis and characterization of poly[3-(2',5'-diheptyloxy-phenyl)thiophene] for use in photoelectron-chemical cells. *Bull. Chem. Soc. Ethiop.* **2007**, 21, 405-417.
3. Li, R.; Fang, Q.; Mou, B.; Chen, M.; Tang, Q.; Shen, B.; Wang, D.; Li, W. A convenient one pot synthesis, crystal structure and chemiluminescence of s,s-diphenyl ethanebis(thioate) compound. *Bull. Chem. Soc. Ethiop.* **2023**, 37, 1185-1191.

4. Foreman, T.K.; Sobol, W.M.; Whitten, D.G. The importance of hydrophobic-hydrophilic factors in binding of charged substrates to micelles: The use of extramicellar probe luminescence to monitor association of cations to the micelle. *J. Am. Chem. Soc.* **1981**, 103, 5333-5336.
5. Yu, H.F.; Chen, K.I.; Yeh, M.H.; Ho, K.C. Effect of trifluoromethyl substituents in benzyl-based viologen on the electrochromic performance: Optical contrast and stability. *Sol. Energy Mater. Sol. Cells* **2019**, 200, 110020.
6. Niu, F.; Zhu, J.L.; Ding, Y.; Tao, L.M.; Jin, J. Energy bands matched photocatalysis enhancement based on viologen derivatives electron-transfer-mediator. *Catal. Sci. Technol.* **2023**, 13, 1640-1649.
7. Lee, J.H.; Youn, C.H.; Kim, B.C.; Gu, M.B. An oxidative stress-specific bacterial cell array chip for toxicity analysis. *Biosens. Bioelectron.* **2007**, 22, 2223-2229.
8. Williams, P.A.; Cosme, J.; Ward, A.; Angove, H.C.; Vinković, D.M.; Jhoti, H. Crystal structure of human cytochrome P450 2C9 with bound warfarin. *Nature* **2003**, 424, 464-468.
9. Seth, S.K.; Sarkar, D.; Jana, A.D.; Kar, T. On the possibility of tuning molecular edges to direct supramolecular self-assembly in coumarin derivatives through cooperative weak forces: Crystallographic and hirshfeld surface analyses. *Cryst. Growth Des.* **2011**, 11, 4837-4849.
10. Bader, F.W.; Slee, T.S.; Cremer, D.; Kraka, E. Description of conjugation and hyperconjugation in terms of electron distributions. *J. Am. Chem. Soc.* **1983**, 105, 5061-5068.
11. Popelier, P.L.A. Characterization of a dihydrogen bond on the basis of the electron density. *J. Phys. Chem. A* **1998**, 102, 1873-1878.
12. Blaney, J. A very short history of structure-based design: How did we get here and where do we need to go? *J. Comput. Aided Mol. Des.* **2012**, 26, 13-14.
13. Higashi, T. *Program for Absorption Correction*, Rigaku Corporation: Tokyo, Japan; **1995**.
14. Sheldrick, G.M. SHELXT – Integrated space-group and crystal-structure determination. *Acta Cryst.* **2015**, A71, 3-8.
15. Sheldrick, G.M. Crystal structure refinement with SHELXL. *Acta Cryst.* **2015**, C71, 3-8.
16. Dolomanov, O.V.; Bourhis, L.J.; Gildea, R.J.; Howarda, J.A.K.; Puschmanna, H. OLEX2: A complete structure solution, refinement and analysis program. *J. Appl. Crystallogr.* **2009**, *42*, 339-341.
17. Brandenburg, K. Putz Gbr, H. *Diamond (Version 3.1c) Crystal and Molecular Structure Visualization*, Crystal Impact: Bonn, Germany; **2004**.
18. Frisch, M.J.; Trucks, G.W.; Schlegel, H.B.; Scuseria, G.E.; Robb, M.A.; Cheeseman, J.R.; Scalmani, G.; Barone, V.; Petersson, G.A.; Nakatsuji, H.; Li, X.; Caricato, M.; Marenich, A. V.; Bloino, J.; Janesko, B.G.; Gomperts, R.; Mennucci, B.; Hratchian, H.P.; Ortiz, J.V.; Izmaylov, A.F.; Sonnenberg, J.L.; Williams-Young, D.; Ding, F.; Lipparini, F.; Egidi, F.; Goings, J.; Peng, B.; Petrone, A.; Henderson, T.; Ranasinghe, D.; Zakrzewski, V.G.; Gao, J.; Rega, N.; Zheng, G.; Liang, W.; Hada, M.; Ehara, M.; Toyota, K.; Fukuda, R.; Hasegawa, J.; Ishida, M.; Nakajima, T.; Honda, Y.; Kitao, O.; Nakai, H.; Vreven, T.; Throssell, K.; Montgomery, J.A.Jr.; Peralta, J.E.; Ogliaro, F.; Bearpark, M.J.; Heyd, J.J.; Brothers, E.N.; Kudin, K.N.; Staroverov, V.N.; Keith, T.A.; Kobayashi, R.; Normand, J.; Raghavachari, K.; Rendell, A.P.; Burant, J.C.; Iyengar, S.S.; Tomasi, J.; Cossi, M.; Millam, J.M.; Klene, M.; Adamo, C.; Cammi, R.; Ochterski, J.W.; Martin, R.L.; Morokuma, K.; Farkas, O.; Foresman, J.B.; Fox, D.J. *Gaussian 16, Revision C.01*, Gaussian, Inc.: Wallingford CT; **2016**.
19. Chai, J.D.; Head-Gordon, M. Systematic optimization of long-range corrected hybrid density functionals. *J. Chem. Phys.* **2008**, 128, 084106.
20. Chai, J.D.; Head-Gordon, M. Long-range corrected hybrid density functionals with damped atom-atom dispersion corrections. *Phys. Chem. Chem. Phys.* **2008**, 10, 6615-6620.
21. Krishnan, R.; Binkley, J.S.; Seeger, R.; Pople, J.A. Self-consistent molecular orbital methods. XX. A basis set for correlated wave functions. *J. Chem. Phys.* **1980**, 72, 650-654.
22. Bernales, V.S.; Marenich, A.V.; Contreras, R.; Cramer, C.J.; Truhlar, D.G. Quantum

mechanical continuum solvation models for ionic liquids. *J. Phys. Chem. B* **2012**, 116, 9122-9129.
23. Lu, T.; Chen, F.W. Multiwfn: A multifunctional wavefunction analyzer. *J. Comput. Chem.* **2012**, 33, 580-592.
24. Spackman, M.A.; Jayatilaka, D. Hirshfeld surface analysis. *Cryst. Eng. Comm.* **2009**, 11, 19-32.
25. Spackman, M.A.; Byrom, P.G. A novel definition of a molecule in a crystal. *Chem. Phys. Lett.* **1997**, 267, 215-220.
26. Turner, M.J.; McKinnon, J.J.; Wolff, S.K.; Grimwood, D.J.; Spackman, P.R.; Jayatilaka, D.; Spackman, M.A. *CrystalExplorer17*, University of Western Australia; **2017**. Available at: http://hirshfeldsurface.net.
27. Yamada, Y.; Okano, J.; Mikami, N. Picosecond IR-UV pump-probe spectroscopic study on the intramolecular vibrational energy redistribution of NH_2 and CH stretching vibrations of jet-cooled aniline. *J. Chem. Phys.* **2005**, 123, 124316.
28. Fukui, K. Role of frontier orbitals in chemical reactions. *Science* **1982**, 218, 747-754.
29. Bader, R.F.W. Atoms in molecules. *Acc. Chem. Res.* **1985**, 18, 9-15.
30. Popelier, P.L.A. Characterization of a dihydrogen bond on the basis of the electron density. *J. Phys. Chem. A* **1998**, 102, 1873-1878.
31. Koch, U.; Popelier, P. Characterization of C-H-O hydrogen bonds on the basis of the charge density. *J. Phys. Chem.* **1995**, 99, 9747-9754.
32. Bader, R.F.W. A bond path: A universal indicator of bonded interactions. *J. Phys. Chem. A* **1998**, 102, 7314-7323.
33. Emamian, S.; Lu, T.; Kruse, H.; Emamian, H. Exploring nature and predicting strength of hydrogen bonds: A correlation analysis between atoms-in-molecules descriptors, binding energies, and energy components of symmetry-adapted perturbation theory. *J. Comput. Chem.* **2019**, 40, 2868-2881.
34. Jenkins, S.; Morrison, I. The chemical character of the intermolecular bonds of seven phases of ice as revealed by ab initio calculation of electron densities. *Chem. Phys. Lett.* **2000**, 317, 97-102.
35. Espinosa, E.; Alkorta, I.; Elguero, J.; Molins, E. From weak to strong interactions: A comprehensive analysis of the topological and energetic properties of the electron density distribution involving X–H···F–Y systems. *J. Chem. Phys.* **2002**, 117, 5529-5542.
36. Dinda, S.; Samuelson, A.G. The nature of bond critical points in dinuclear copper(I) complexes. *Chem. Eur. J.* **2012**, 18, 3032-3042.
37. Roy, S.; Rhim, J.W. Probing the binding interaction of lysozyme-viologen herbicide. *J. Mol. Struct.* **2018**, 1171, 1-8.
38. Das, A.; Thakur, R.; Dagar, A.; Chakraborty, A. A spectroscopic investigation and molecular docking study on the interaction of hen egg white lysozyme with liposomes of saturated and unsaturated phosphocholines probed by an anticancer drug ellipticine, *Phys. Chem. Chem. Phys.* **2014**, 16, 5368-5381.
39. Khan, A.Y.; Kumar, G.S. Natural isoquinoline alkaloids: Binding aspects to functional proteins, serum albumins, hemoglobin, and lysozyme. *Biophys. Rev.* **2015**, 7, 407-420.
40. Morris, G.M.; Huey, R.; Lindstrom, W.; Sanner, M.F.; Belew, R.K.; Goodsell, D.S.; Olson, A.J. Autodock4 and AutoDockTools4: Automated docking with selective receptor flexiblity. *J. Comput. Chem.* **2009**, 16, 2785-2791.
41. DeLano, W.L. The PyMOL molecular graphics system, **2002**. Available at: https://github.com/schrodinger/pymol-open-source
42. Chamani, J.; Tafrishi, N.; Momen-Heravi, M. Characterization of the interaction between human lactoferrin and lomefloxacin at physiological condition: multi- spectroscopic and modeling description. *J. Lumin.* **2010**, 130, 1160-1168.